Supporting Information for

Innovative Lithium Storage Enhancement in Cation-Deficient Anatase via Layered Oxide Hydrothermal Transformation

Fengqi Lu[1], Qiang Chen[1], Shipeng Geng[1], Mathieu Allix[2], Hui Wu[3], Qingzhen Huang[3], Xiaojun Kuang[1]*

1. MOE Key Laboratory of New Processing Technology for Nonferrous Metal and Materials, Guangxi Universities Key Laboratory of Nonferrous Metal Oxide Electronic Functional Materials and Devices, College of Materials Science and Engineering, Guilin University of Technology, Guilin 541004, P. R. China.

2. UPR3079 CEMHTI, 1D Avenue de la Recherche Scientifique, 45071 Orléans Cedex 2, and Université d'Orléans, Faculté des Sciences, Avenue du Parc Floral, 45067 Orléans Cedex 2, France

3. NIST Center for Neutron Research, National Institute of Standards and Technology, Gaithersburg, Maryland 20899, United States.

E-mail: kuangxj@glut.edu.cn， Tel.: +86-0773-5896670

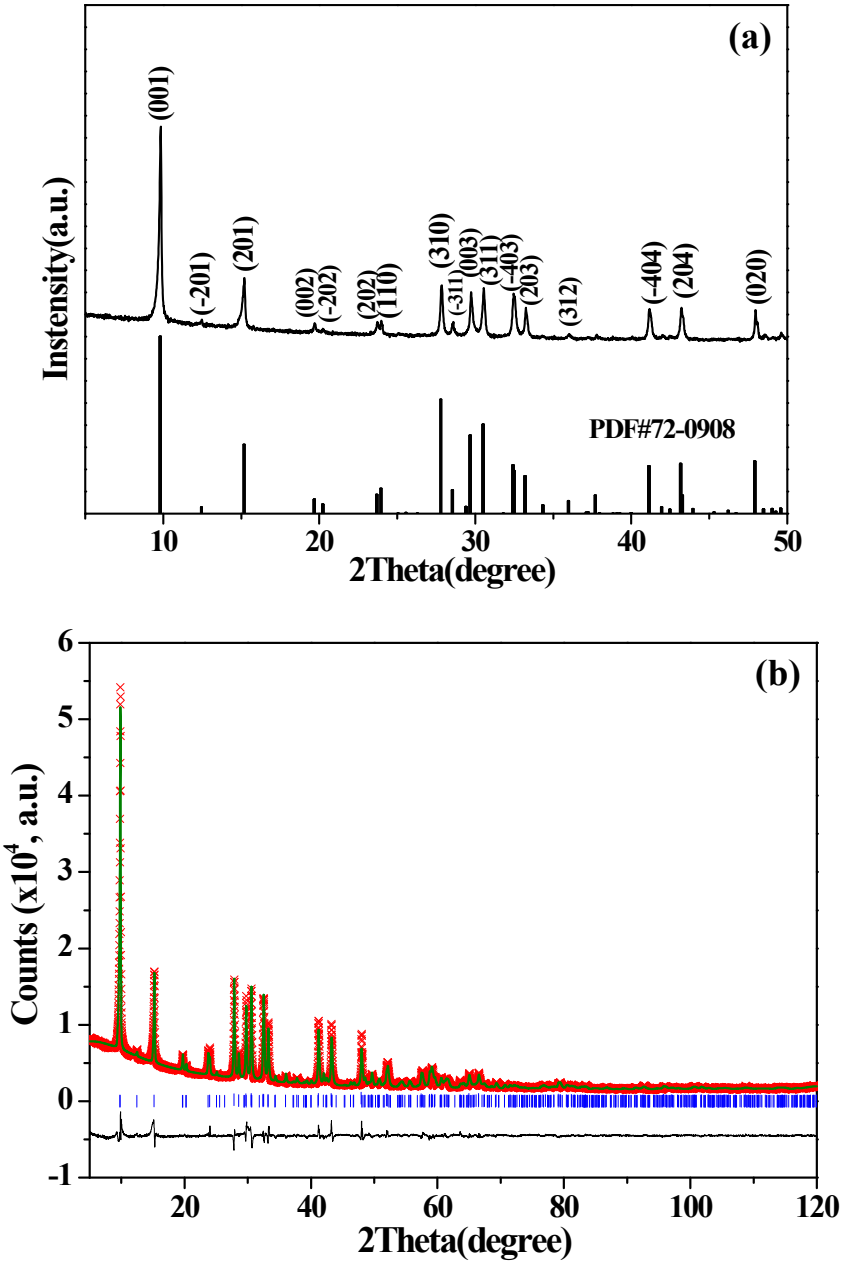

Figure S1. XRD pattern (a) and Rietveld refinement (b) of $K_3Ti_5NbO_{14}$. The reliability factors of refinement are R_{wp} ~ 5.30% and R_p ~ 3.66%.

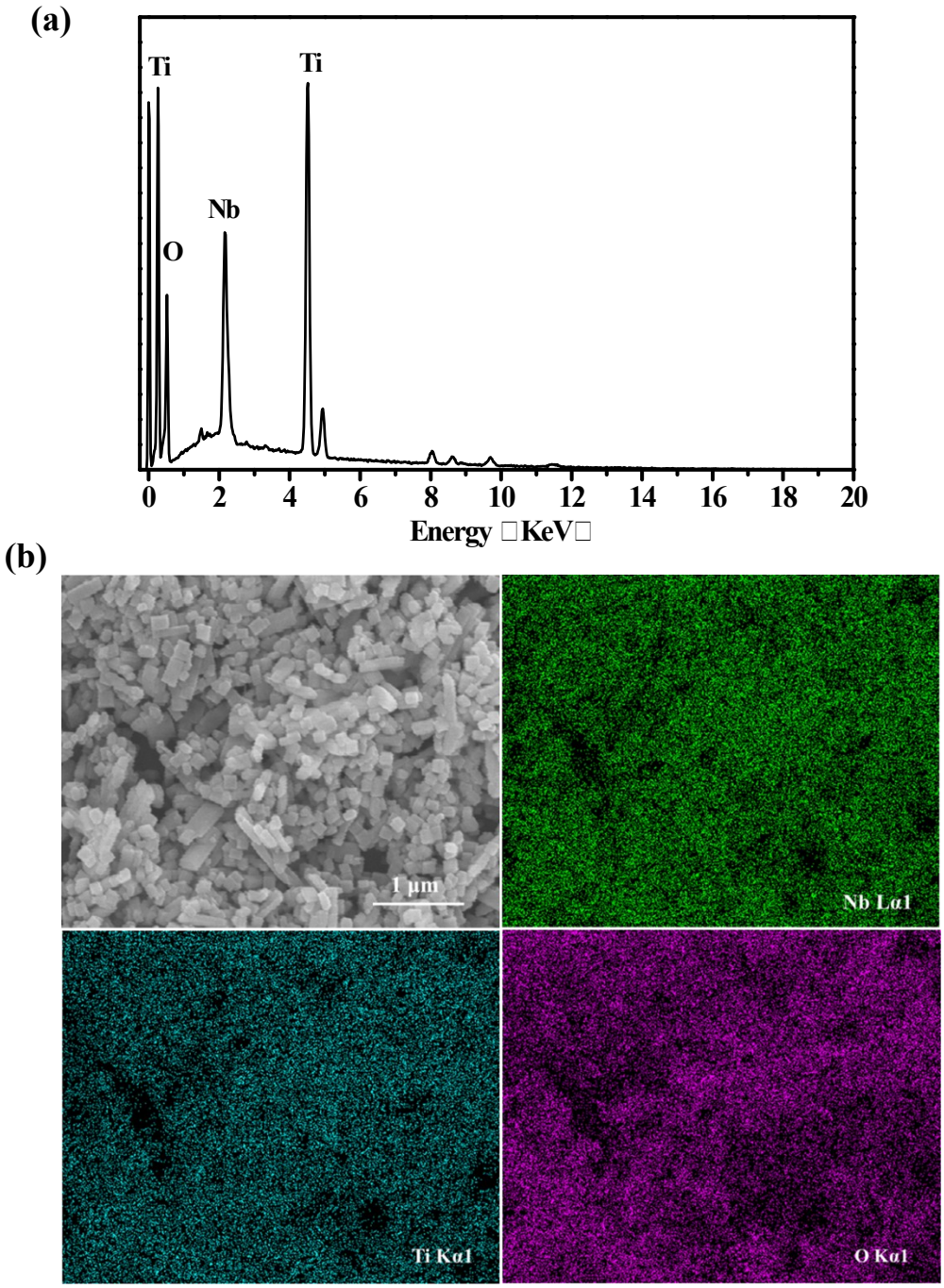

Figure S2. (a) EDS spectrum of TNO synthesized at 0.5 M acetic acid treatment at 180 ºC for 96 h under hydrothermal. (b) EDS elemental mapping images of Nb, Ti, and O elements in NTO samples.

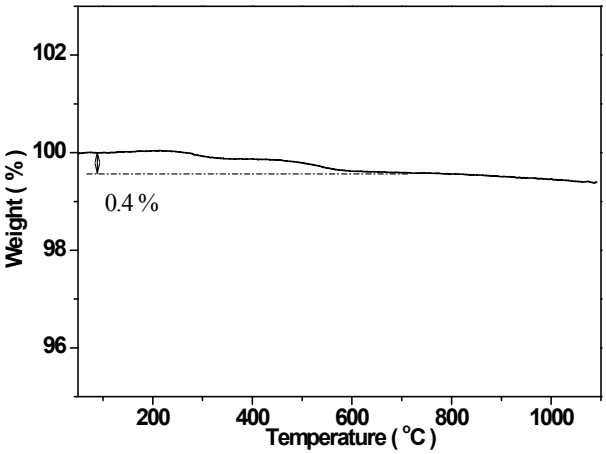

Figure S3. TG curve of the sample after 0.5 M acetic acid treatment at 180 ºC for 48 h under hydrothermal condition.

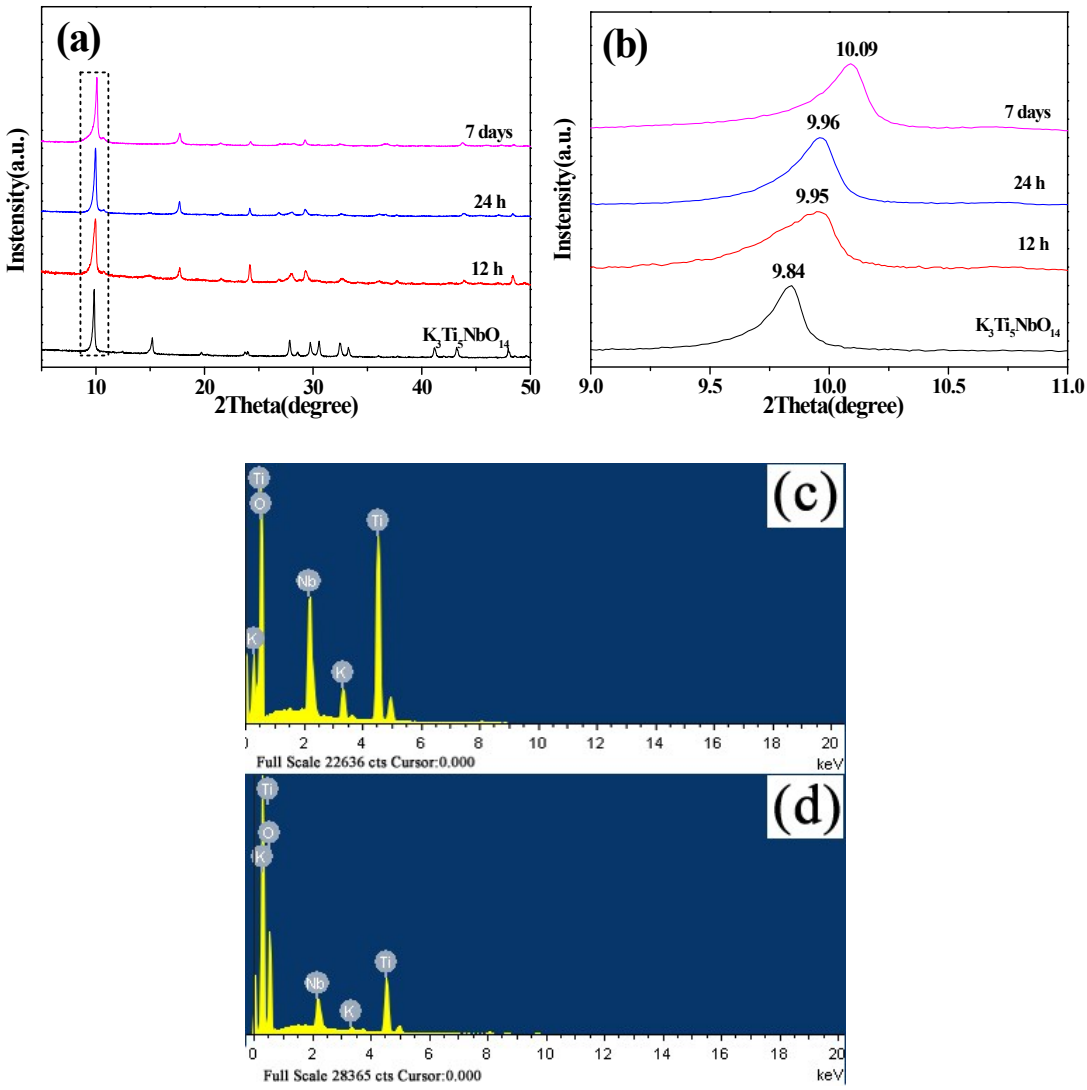

Figure S4. (a) X-ray diffraction patterns of $K_3Ti_5NbO_{14}$ at 0.5 M acetic acid treatment at various times at ambient temperature; (b) partial enlargement of (a). EDS spectrum of $K_3Ti_5NbO_{14}$ after acetic acid treatment at ambient temperature at (c) 24 h and (d) 7 days.

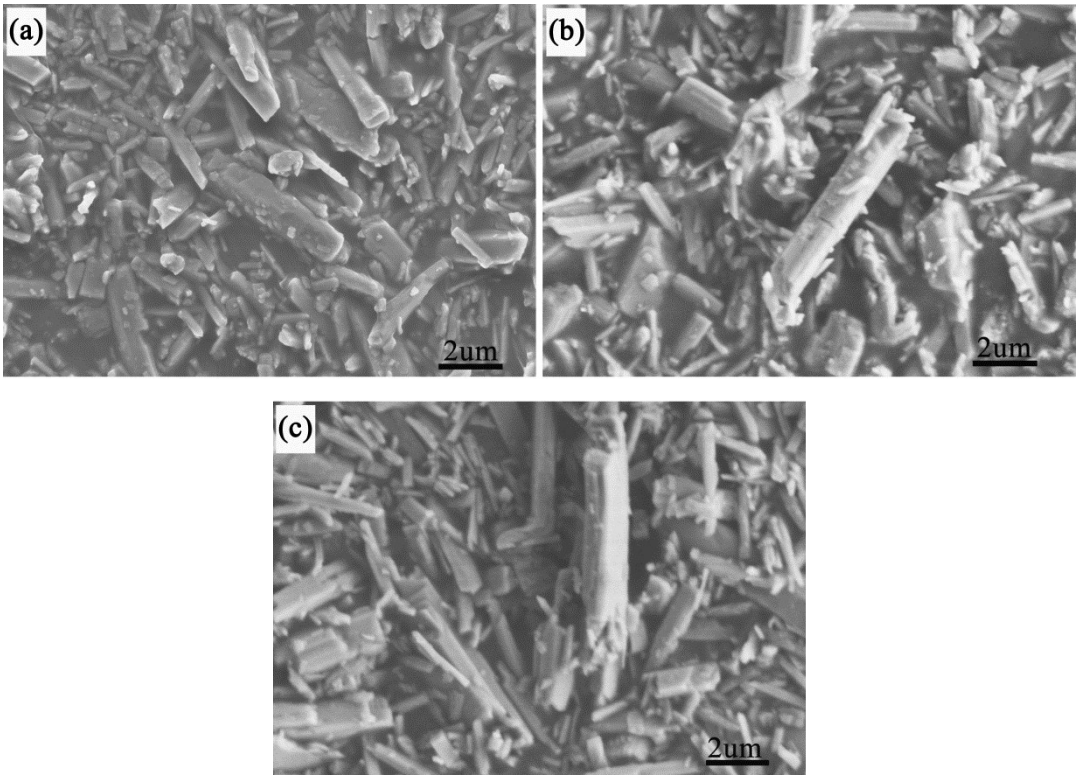

Figure S5. SEM image of $K_3Ti_5NbO_{14}$ after 0.5 M acetic acid treatment at various times at ambient temperature: (a) 12 h, (c) 24 h, (d) 7 days.

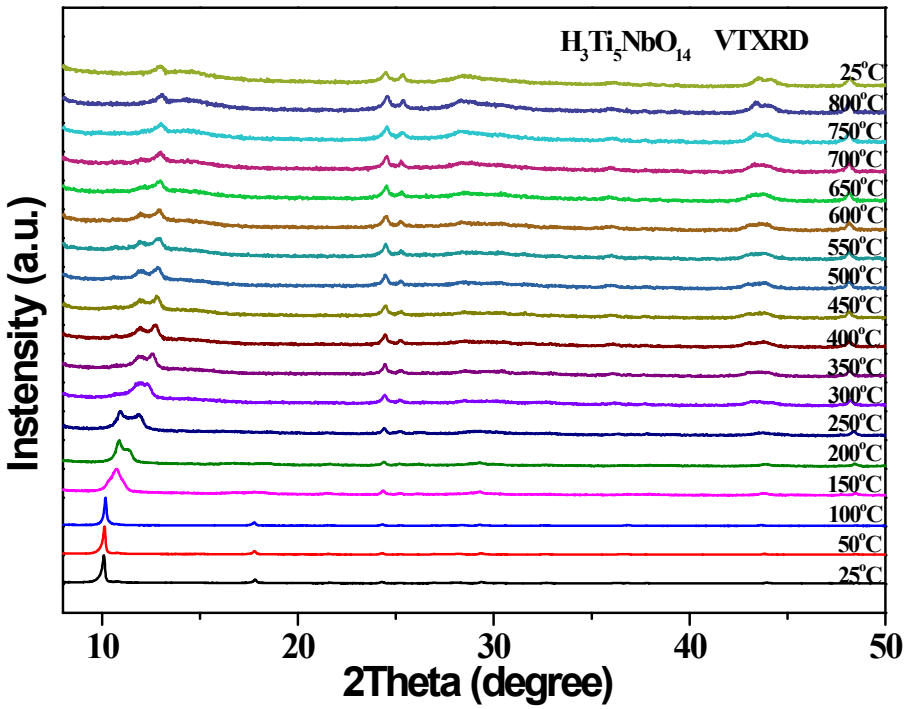

Figure S6. VT-XRD patterns of $K_3Ti_5NbO_{14}$ after 0.5 M acetic acid treatment for 7 days at ambient temperature.

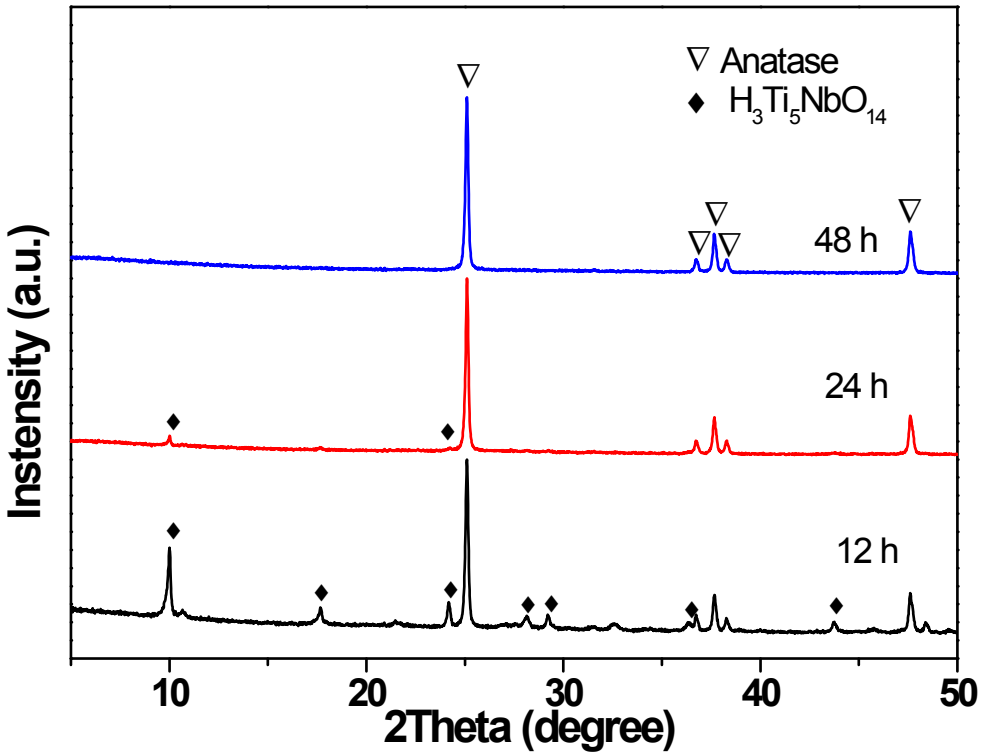

Figure S7. XRD patterns of $K_3Ti_5NbO_{14}$ after 1 M acetic acid treatment at 180 ºC for various times under hydrothermal condition.

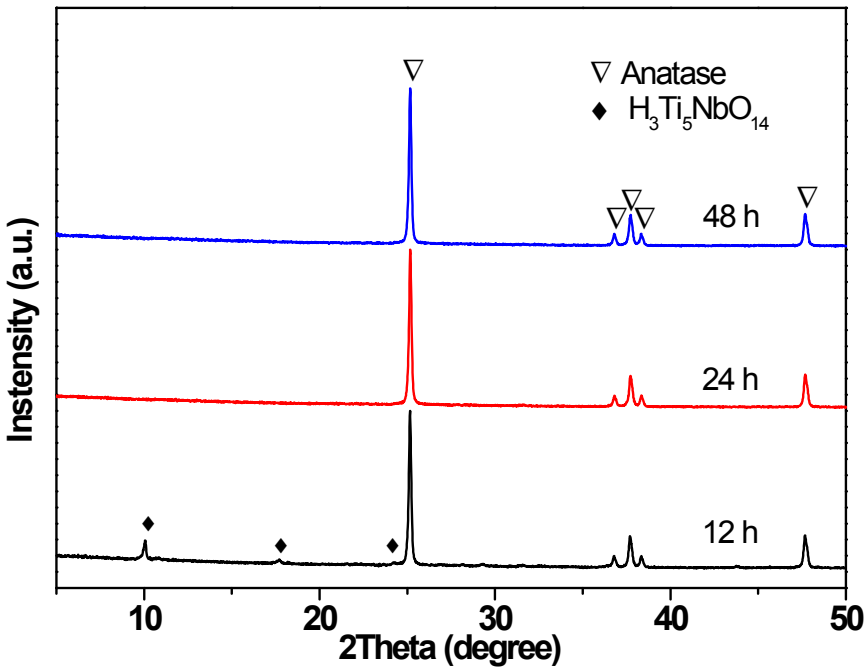

Figure S8. XRD patterns of $K_3Ti_5NbO_{14}$ after 5 M acetic acid treatment at 180 ºC for various times under hydrothermal condition.

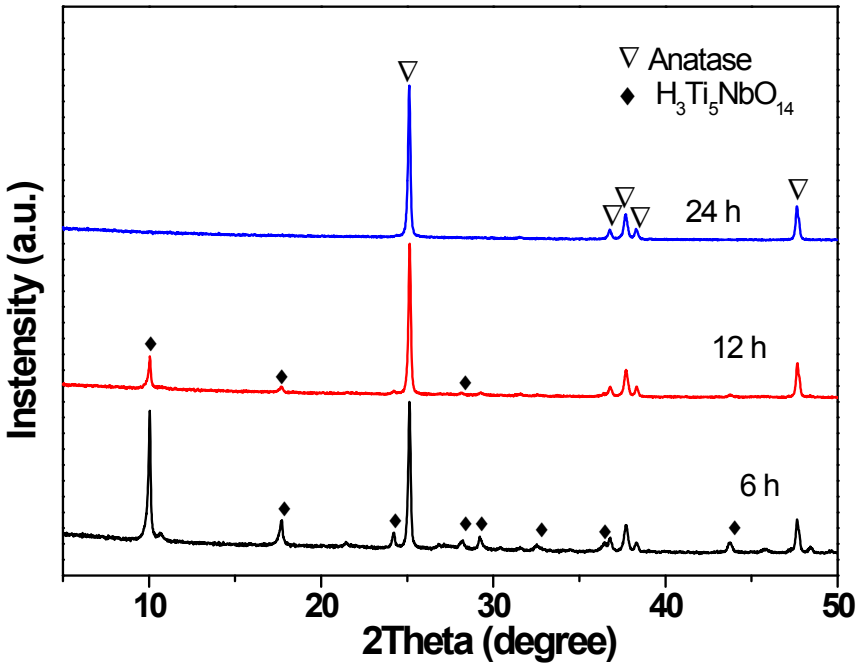

Figure S9. XRD patterns of $K_3Ti_5NbO_{14}$ after 10 M acetic acid treatment at 180 ºC for various times under hydrothermal condition.

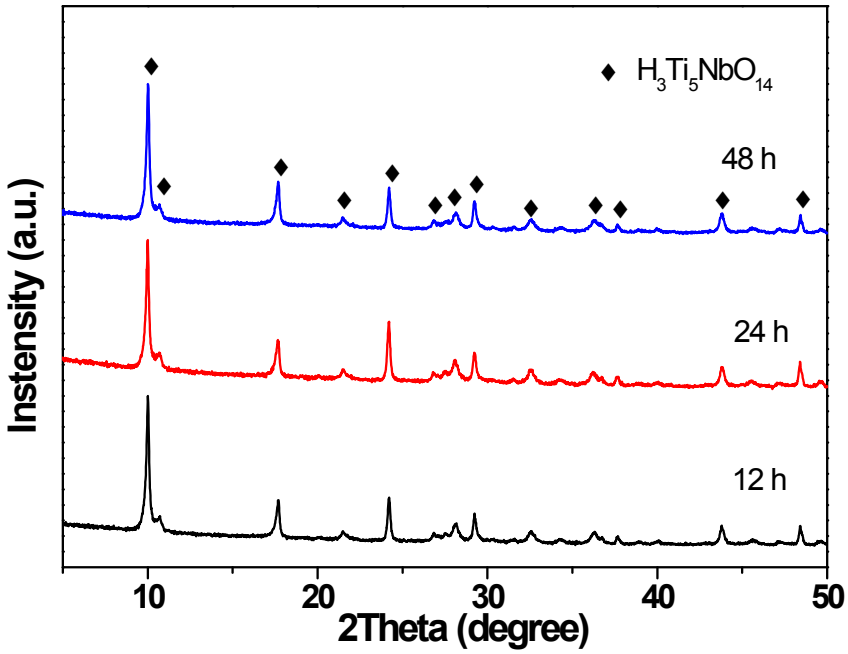

Figure S10. XRD patterns of $K_3Ti_5NbO_{14}$ after 17.4 M acetic acid treatment at 180 ºC for various times under hydrothermal condition.

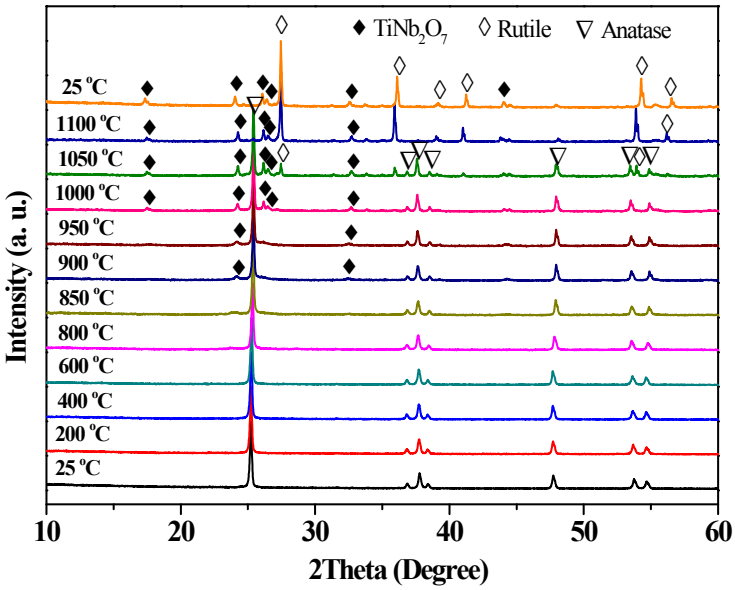

Figure S11. In situ VT-XRD profiles of NTO from 25 to 1100 °C.

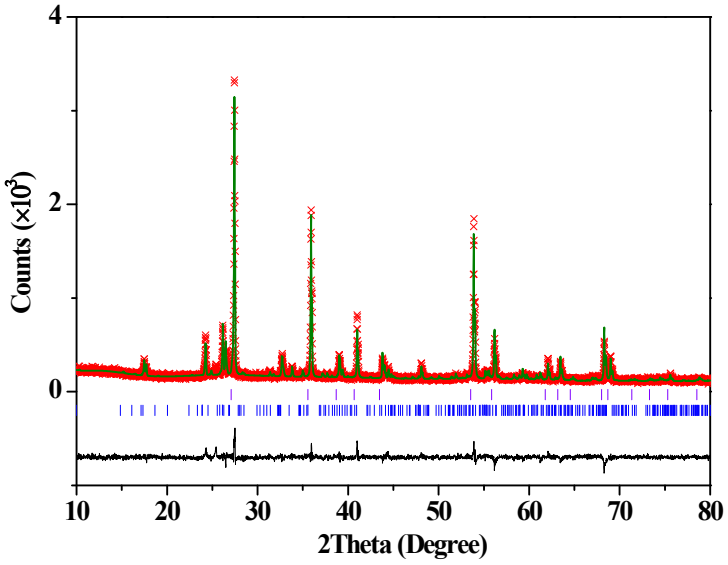

Figure S12. Rietveld refinement of room temperature XRD data of the NTO samples after VT-XRD experiment up to 1100 °C. The reliability factors were R_{wp} ~ 9.15 %, R_p ~ 7.11 %. The two rows of vertical ticks denote the Bragg reflection positions of rutile TiO_2 (top, ~ 71.6 wt%, space group: $P4_2/mnm$, $a = b = 4.6523(1)$ Å, $c = 3.0009(1)$ Å) and $TiNb_2O_{17}$ (bottom, ~ 28.4 wt%, space group: $C2/m$, $a = 20.5069(9)$ Å, $b = 3.8054(1)$ Å, $c = 11.9845(6)$ Å).

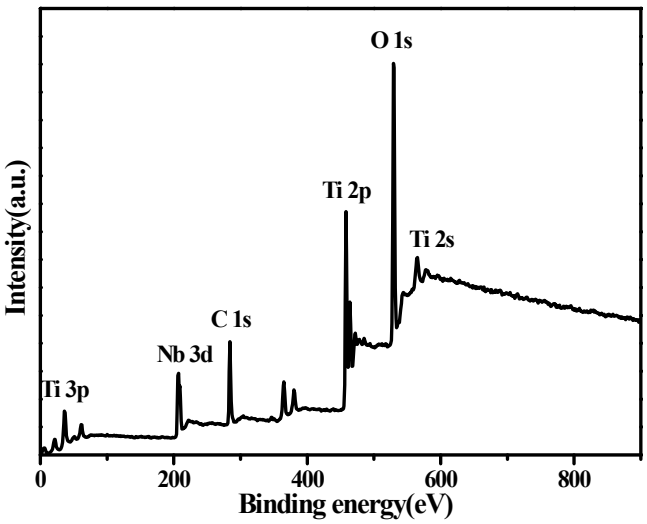

Figure S13. XPS spectra of the survey scan for the NTO nanoparticles.

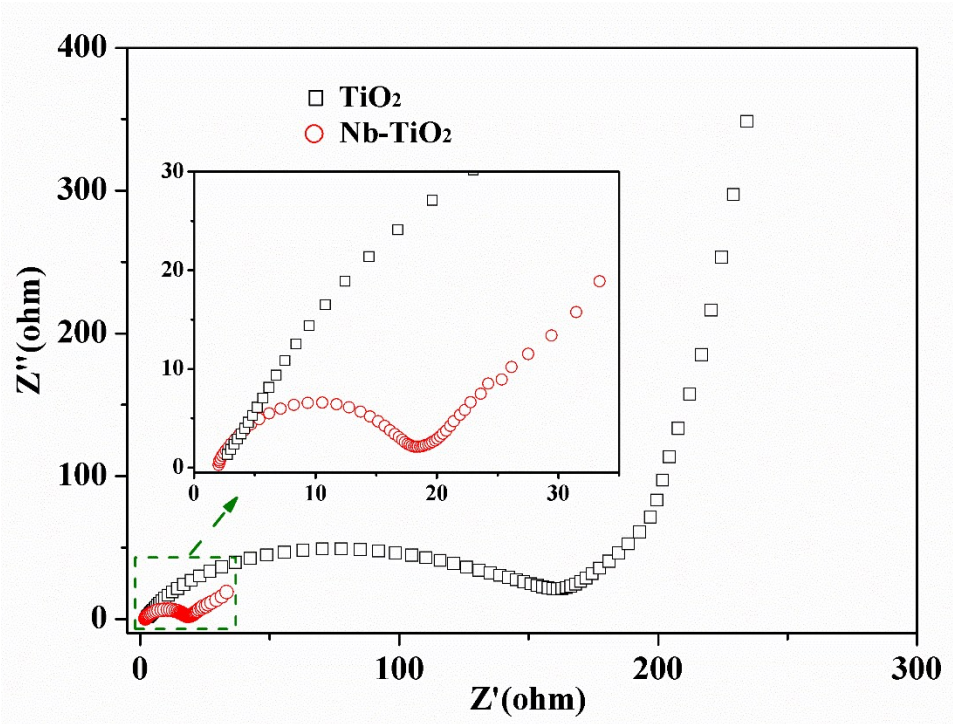

Figure S14. The Nyquist plots of NTO and commercial anatase TiO_2 electrodes.

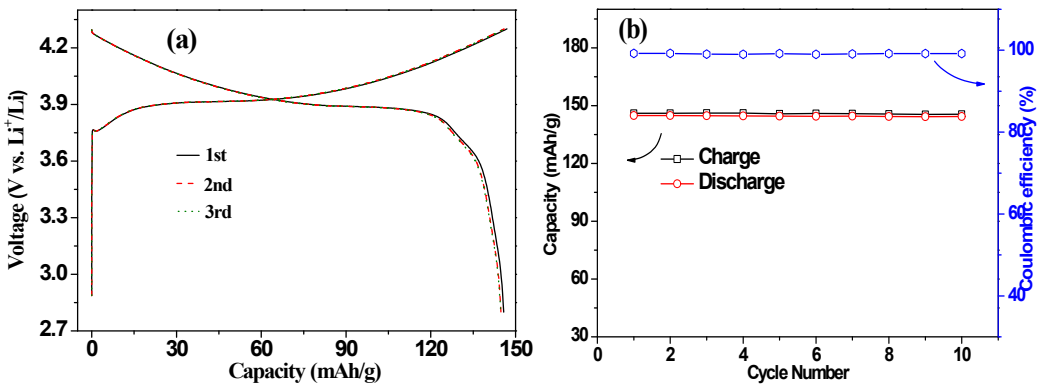

Figure S15. Electrochemical performances of $LiCoO_2$: (a) galvanostatic charge-discharge voltage curves at 0.1 C (1 C = 150 mA/g) in the 2.8-4.3 V voltage range, (b) cyclic performance.

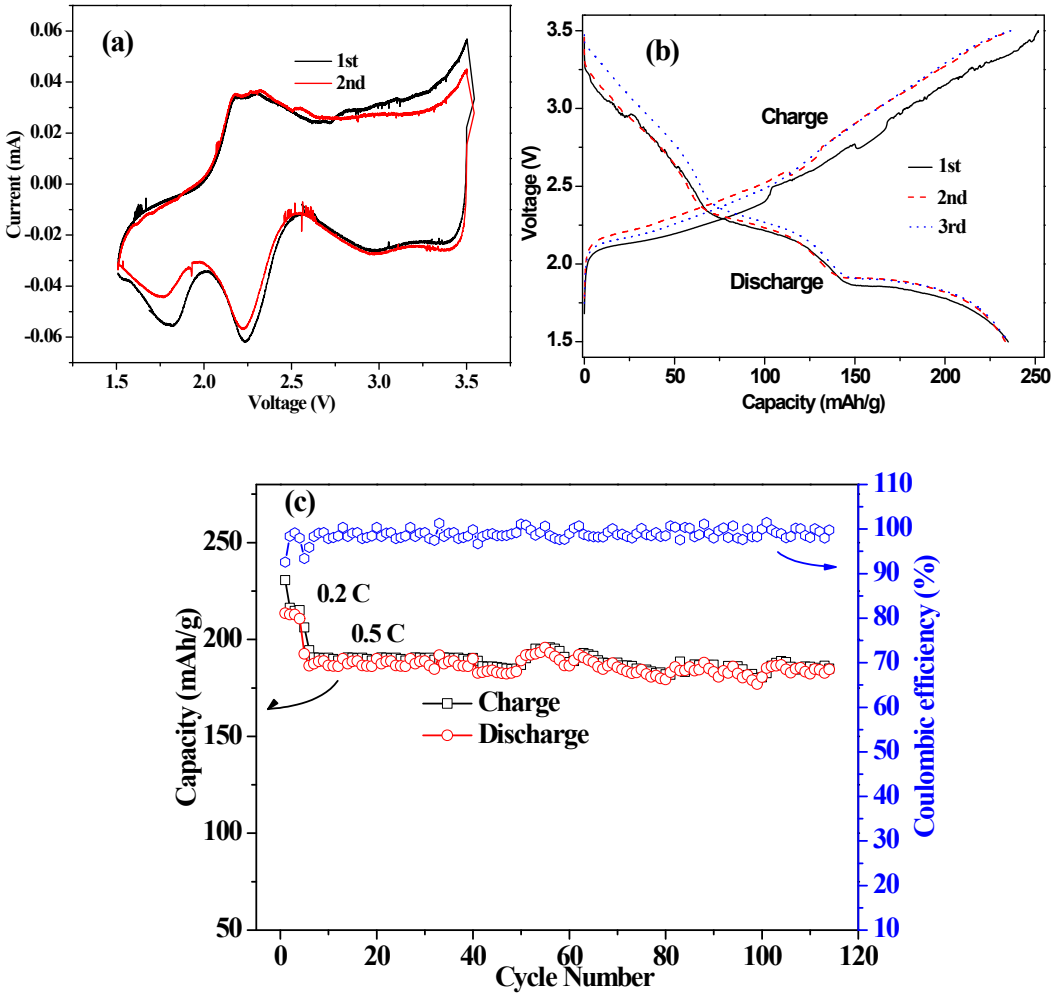

Figure S16. Electrochemical performance of the NTO//LCO full cell: (a) cyclic voltammetry curves for the 1st and 2nd cycle for the NTO//LCO full cell at a scan rate of 0.2 mV/s, (b) voltage-capacity curves of the NTO//LCO full cell, (c) cycling performances of the NTO//LCO full cell at a current density of 0.5 C in the 1.5-3.5 V voltage range.

Table S1. Comparison of the performance of NTO//LCO full cell with some TiO_2-based full cell in previous literatures.

Positive electrode	Negative electrode	Working potential	Current density	Discharge capacity (mAh/g)	Ref.
$LiCoO_2$	Nb-doped TiO_2 anatase	2.3 V	0.2 C	230.2 15 cycles	This work
$LiFePO_4$/C	anatase TiO_2/graphene	1.6 V	1 C	125 700 cycles	46
$LiMn_2O_4$	anatase TiO_2	2.1 V	150 mA/g	104 100 cycles	47
$LiNi_{0.5}Mn_{1.5}O_4$	anatase TiO_2	2.8 V	0.1 C	87 400 cycles	48
$LiFePO_4$	rutile TiO_2	1.8 V	C/3	70 40 cycles	49
$LiMn_2O_4$	TiO_2(B)	2.5 V	150 mA/g	89 1000 cycles	50
$LiCoO_2$	anatase TiO_x	2.2 V	0.5 C	108 100 cycles	51
$LiNi_{0.5}Mn_{1.5}O_4$	amorphous TiO_2	2.8 V	16 mA/g	310 25 cycles	52

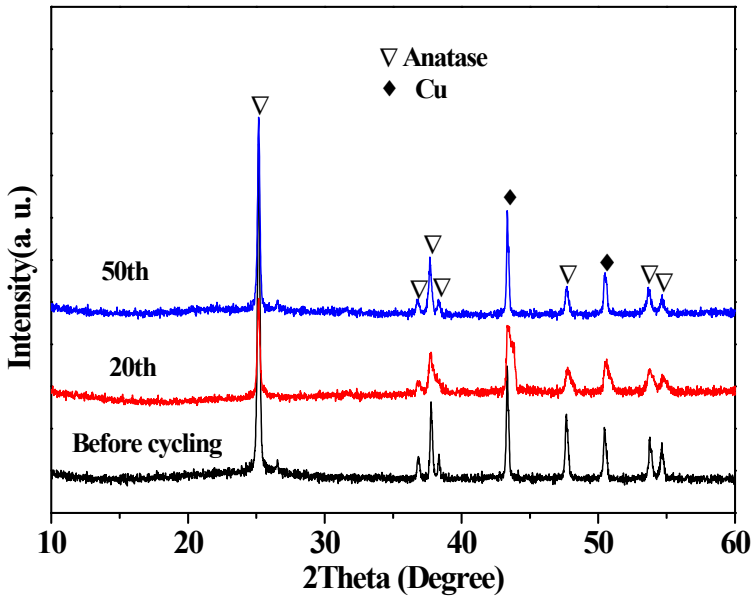

Figure S17. XRD patterns of NTO electrodes before charge-discharge cycling and after the 20th and 50th cycles at the current density of 0.2 C. The diffraction peaks of Cu come from the Cu foil current collector.

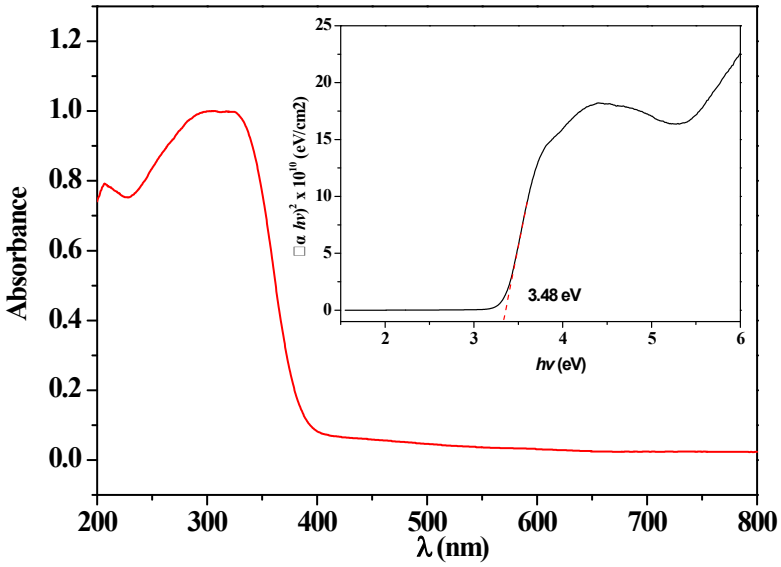

Figure S18. UV-vis light absorption spectrum of NTO. The inset shows plots of $(ahv)^2$ vs energy *hv* for NTO, from which the estimated band gaps (eV) is ~ 3.48 eV.

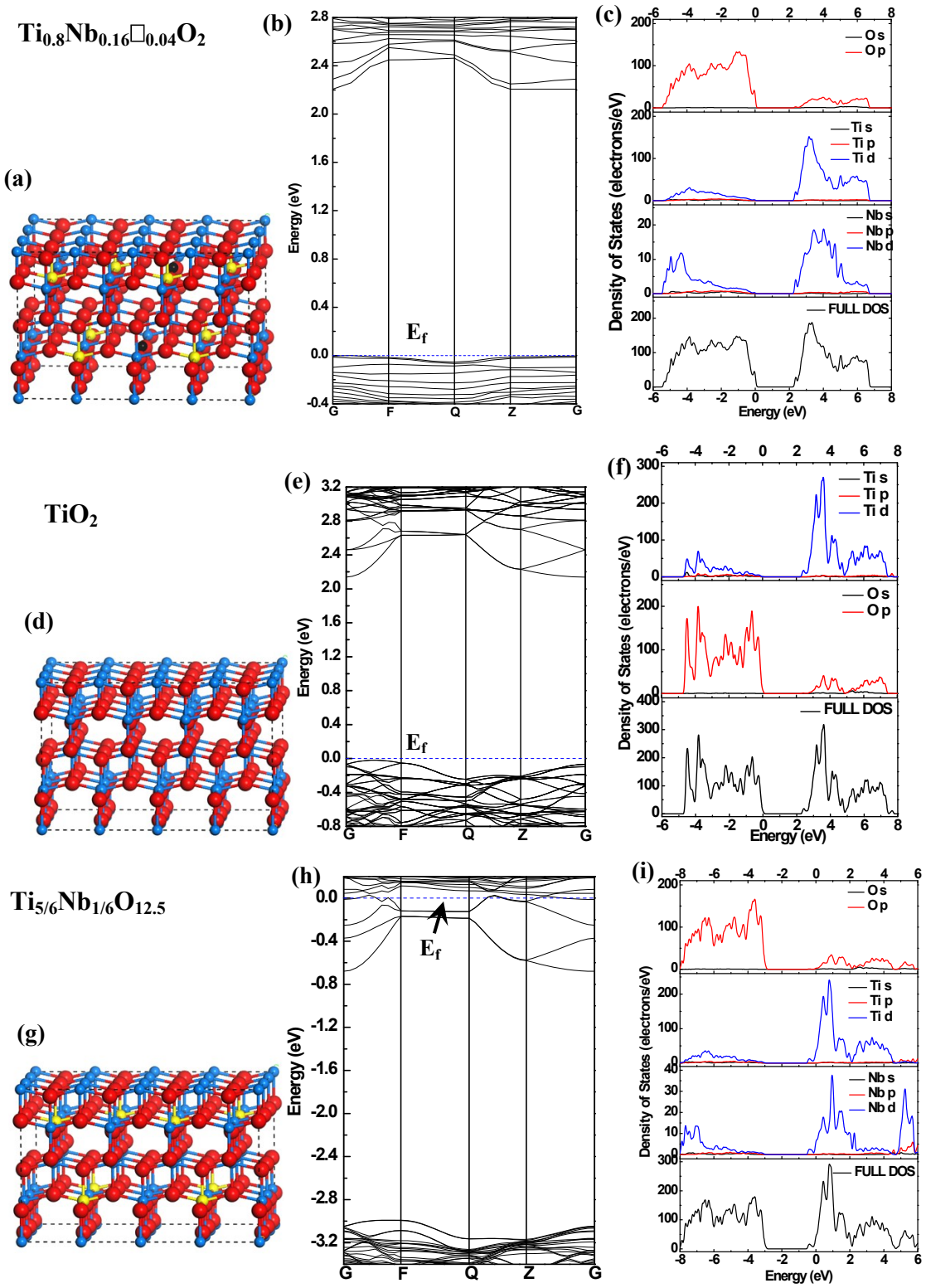

Figure S19. Structural models, band structures, and total and partial density of states for (a-c) cation-deficient anatase $Ti_{0.8}Nb_{0.16}\square_{0.04}O_2$, (d-f) undoped anatase TiO_2 and (g-i) cationic-site fully-occupied $Ti_{5/6}Nb_{1/6}O_2$. The spheres in dark cyan, yellow, red and black denote the Ti, Nb and O atoms and vacant site, respectively. The impurity Nb atoms and vacancies are distributed apart from each other without sharing oxygen atoms. The blue dash lines denote the Fermi levels (E_f).